

KHAN, U.H., BASIT, A., KHAN, W., JADOON, M.A.K. and BAIG, N.A. 2024. Cognitive dual coprime frequency diverse array MIMO radar network for target discrimination and main-lobe interference mitigation. *IET radar, sonar and navigation* [online], 18(9), pages 1584-1597. Available from: <https://doi.org/10.1049/rsn2.12595>

# Cognitive dual coprime frequency diverse array MIMO radar network for target discrimination and main-lobe interference mitigation.


KHAN, U.H., BASIT, A., KHAN, W., JADOON, M.A.K. and BAIG, N.A.

2024

© 2024 The Author(s). *IET Radar, Sonar & Navigation* published by John Wiley & Sons Ltd on behalf of The Institution of Engineering and Technology. This is an open access article under the terms of the Creative Commons Attribution License, which permits use, distribution and reproduction in any medium, provided the original work is properly cited.

## ORIGINAL RESEARCH

# Cognitive dual coprime frequency diverse array MIMO radar network for target discrimination and main-lobe interference mitigation

Umair Hafeez Khan<sup>1</sup>  | Abdul Basit<sup>1</sup> | Wasim Khan<sup>1</sup> |  
Muhammad Adeel Khan Jadoon<sup>1</sup> | Nauman Anwar Baig<sup>2</sup>

<sup>1</sup>Department of Electrical and Computer Engineering, International Islamic University, Islamabad, Pakistan

<sup>2</sup>Department of Electronic and Electrical Engineering, School of Engineering, Robert Gordon University, Aberdeen, Scotland

**Correspondence**

Nauman Anwar Baig  
Email: [N.baig@rgu.ac.uk](mailto:N.baig@rgu.ac.uk)

**Funding information**

Robert Gordon University

**Abstract**

The authors propose a novel dual coprime frequency diverse array (FDA) multiple input multiple output (DCFDA-MIMO) radar network design, empowered by cognitive capabilities, aimed at target discrimination and mitigation of interference present in the standalone radar systems. That is, the proposed DCFDA-MIMO design capitalises on the complementary advantages of FDAs for target discrimination and coprime arrays for enhanced resolution, resulting in superior performance. Additionally, the proposed DCFDA-MIMO network employs a 2D multiple signal classification algorithm to achieve high-resolution target localisation. By incorporating cognitive techniques based on the action-perception cycle, the proposed approach demonstrates notable improvements in multiple target detection and tracking accuracy with fewer number of antenna elements as compared to existing techniques. Furthermore, it enhances individual radar beamforming performance for interference suppression and true target detection without prior information.

**KEYWORDS**

antenna arrays, MIMO radar, phased array radar, radar

## 1 | INTRODUCTION

The applications of radar technology are diverse, yet its use in defence remains widely recognised. Notably, accurate and efficient target detection and tracking has captivated researchers for decades. Various antenna array configurations and detection algorithms have been employed to enhance radar tracking performance, generally, focusing on single and multiple targets in the dense interference scenarios. Nevertheless, dedicated efforts have also been directed towards improving antenna arrays structures and signal processing algorithms to ensure accurate detection and tracking amidst interference.

On the antenna front, phased arrays, boasting multiple transmit antennas and phase shifters, have been in use for over two decades. They electronically steer the beam by leveraging constructive and destructive interference to focus the emission

in a specific direction, albeit only in the angular dimension. This results in a highly directional beam with nulls generated elsewhere [1–3]. Moreover, building upon Phased-MIMO, which introduced spatial diversity by dividing the array into subarrays, better angular resolution was achieved [4]. However, these techniques lacked range dependence in its transmitted beam. Note that, this limitation was addressed by Antonik et-al by introducing the Frequency Diverse Arrays (FDA), which utilise a small frequency increment between antenna elements to generate a transmitted beam pattern dependent on both angle and range. This advancement attracted attention due to its superior target detection and tracking capabilities [5, 6]. Unlike Phased Arrays, FDA can identify two distinct targets within the same angle but at different ranges [7]. Further improvements came from combining FDA with MIMO, leveraging the spatial diversity of MIMO while maintaining the range-dependent

This is an open access article under the terms of the [Creative Commons Attribution](https://creativecommons.org/licenses/by/4.0/) License, which permits use, distribution and reproduction in any medium, provided the original work is properly cited.

© 2024 The Author(s). *IET Radar, Sonar & Navigation* published by John Wiley & Sons Ltd on behalf of The Institution of Engineering and Technology.

advantage of FDA [8, 9]. Additionally, a recent development in array structures has introduced a novel type of array called Coprime Arrays. These arrays utilise sets of elements with coprime integer numbers in both the transmitter and receiver configurations that allows detection of more number of targets with fewer antenna elements compared to the conventional arrays [10, 11]. Therefore, combining Coprime Arrays with FDA yields an array capable of detecting even more targets with fewer elements, while maintaining the benefits of both angle and range-dependent beams [12].

Furthermore, the integration of cognitive radar features into target detection and tracking has emerged as a recent area of intense research interest, fuelled by the growing desire for autonomous radar systems. Note that, the cognitive perception-action cycle aligns with the booming field of artificial intelligence (AI) and its potential applications to radar technology. The seminal work by Haykin (2006) drew inspiration from bats' natural navigation, highlighting the concept of a 'cognitive radar system' [13].

Beyond conceptualisation, various applications of cognitive functionalities have been actively explored and implemented in radar systems, as evidenced by the work of Martone (2014) and others [14]. Similarly, diverse cognitive radar architectures have been proposed and discussed in literature, such as those outlined by Guerci (2010) [15] etc. One notable example involves harnessing deep learning for integrated target classification and revisit time calculation within a hybrid cognitive radar architecture, as demonstrated by Sagayaraj et al. (2018) [16]. Additionally, AI integration has enabled automatic decision-making capabilities, exemplified by element-wise power control in spectrally dense environments, as explored by Nusenu et al. (2018) and Ding et al. (2023) [17] [18].

Real-world environments often throw curveballs at radars, including intentional interference designed to degrade performance and lose track of targets. One such tactic is Digital Radio Frequency Memory (DRFM), which captures the radar's emitted signal and rebroadcasts it, effectively confusing the radar into mistaking the echo for a real target and compromising its estimates [19, 20]. Researchers have risen to this challenge, proposing various countermeasures. Some methods focus on transforming the transmitted signal to make it harder to replicate, as explored by Zhong et al. (2018) and Wei et al. (2016) [21, 22]. Next, others investigate modifying antenna array configurations to cancel the jamming effect, as seen in Yang et al.'s (2023) work on cognitive radar [23]. Additionally, signal processing techniques at the receiver end offer another line of defence, as demonstrated by Xu et al. (2015) [24].

Lan et al. (2020) [25] demonstrated a technique to broaden the null region through the introduction of artificial interference, enhancing its resilience to errors and ensuring superior suppression of deceptive jammers. Additionally, Lan et al. (2023) [26] proposed a method that combines transmit and receive beamforming to broaden the mainlobe, resulting in a beampattern with a robust, flat mainlobe for the desired signal while maintaining deep nulls for interference suppression. Furthermore, Lan et al. (2020) [27] presented three distinct approaches utilising mathematical optimisation, discrete grid

search, and the Newton method as detectors within the FDA-MIMO framework to enhance target detection. Alternatively, Gong et al. [28–30] investigate strategies to diminish the detectability of a radar system by reducing its low probability of intercept through minimising the power footprint in clustered environments.

In this paper, we tackle the challenge of robustly detecting and tracking multiple targets amidst interference, particularly, the main lobe interference likewise the DRFM. We propose a novel Dual Coprime FDA-Multiple Input and Output (DCFDA-MIMO) radar network, empowered by cognitive capabilities, for an improved true target/targets detection, localisation and tracking performance. Note that, the proposed design of a DCFDA-MIMO network represents a unique contribution as it offers superior resolution and robust detection of multiple targets with fewer antenna elements of DCFDA than that of the existing techniques and hasn't been explored yet in literature.

The proposed method involves a dual-stage approach for detecting and tracking multiple targets, harnessing cognitive capabilities to ensure dependable results.

The proposed design capitalises on:

- The strengths of FDA's target discrimination and the coprime array's enhanced resolution have been utilised to improve the overall design's performance.
- It employs a Search-Discrimination-Initialisation technique, which leverages target distribution characteristics and deceptive trajectory interference to discriminate between true targets and interferences across various radars in the network.
- The DCFDA-MIMO network utilises a 2D multiple signal classification (MUSIC) algorithm for acquiring true target localisation, aided by a distance matrix derived from the inputs of multiple radars.

Finally, leveraging the perception-action cycle, our design delivers a substantial boost in multi-target detection and tracking accuracy. Furthermore, it optimises individual radar beamforming, while effectively mitigates interference to ensure precise detection of unseen targets.

The paper is distributed as follows, section-2 presenting preliminary knowledge followed by section-3 describes the system model, followed by describing the target model, followed by detection and targeting methodology in section 4. Moreover, Experiment, Results and Conclusion are given in section 5 and 6, respectively.

## 2 | PRELIMINARY KNOWLEDGE

### 2.1 | Frequency diverse array

Recent innovation in radar technology, the FDA (FDA), leverages subtle frequency variations across its elements to achieve precise 3D target localisation. This unlocks a range of powerful applications, including high-accuracy tracking, interference

suppression, and effective target identification in complex environments with clutter. A uniform linear array of  $M$  elements with frequency increments  $\Delta f$  between them is shown in Figure 1, where  $X$  is the axis on which the array is established.

FDA stands out from conventional phased arrays by employing a key difference: minute frequency variations across its elements. This distinctive feature not only shapes its received signal model but also empowers its remarkable ability to pinpoint targets in three dimensions which is given as follows:

$$\mathbf{x}(t, \tau) = \sum_{l=1}^L \alpha_l(\tau) \left[ (\mathbf{W}^H \mathbf{a}(\theta_l, r_l))^T \boldsymbol{\phi}_K(t) \right] \mathbf{b}(\theta_l) + \mathbf{n}(t, \tau) \quad (1)$$

where  $\tau$  is the time delay (azimuth time),  $\alpha_l(\tau)$  is the target reflection coefficient and  $\mathbf{n}(t, \tau)$  is the Gaussian noise. Whereas, transmit and receive steering vector is given as follows:

$$\mathbf{b}(\theta) = \left[ 1, e^{-j\left(\frac{2\pi f_0 d \sin \theta}{c_0}\right)}, \dots, e^{-j\left(\frac{2\pi f_0 (N-1)d \sin \theta}{c_0}\right)} \right]^T \quad (2)$$

$$\mathbf{a}(r, \theta) = \left[ 1, e^{-j\Theta(r, \theta)}, \dots, e^{-j\Theta(r, \theta)} \right]^T \quad (3)$$

where  $T$  denotes the transpose operator and  $\Theta(r, \theta)$  is written as follows:

$$\Theta(r, \theta) = \frac{2\pi[(f_0 d \sin \theta + \Delta f d \sin \theta) - \Delta f r]}{c_0} \quad (4)$$

where  $f_0$  denotes the operational frequency,  $r$  denotes range,  $\Delta f$  represents the frequency increment between the elements,  $\theta$  denotes the angle with respect to boresight and  $d = \frac{\lambda}{2}$  where  $\lambda = \frac{c}{f_0}$  and  $c$  is the speed of light which is  $3 \times 10^8$  m/s.

## 2.2 | FDA-MIMO

Fusing the strengths of FDAs (FDA) and MIMO arrays, FDA-MIMO leverages FDA's range resolution and MIMO's waveform diversity to offer enhanced capabilities. In this setup,  $M$  transmitting elements and  $N$  receiving antennas collaborate to receive a baseband signal as given below [31].

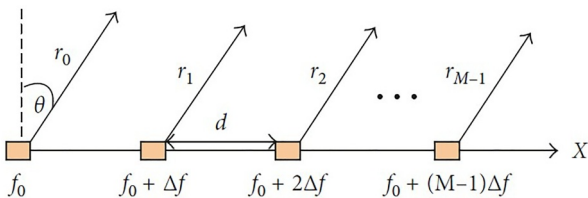


FIGURE 1 Frequency diverse array (FDA) [7].

$$\begin{aligned} \mathbf{r}_{FM}(t) &= \mathbf{a}\mathbf{b}(\theta) \left[ \mathbf{W}_{FM}^H \mathbf{a}(\theta, r) \right] \boldsymbol{\phi}_{FM}(t - \tau) + \mathbf{n}(t) \\ &= \mathbf{s}_{FM} + \mathbf{n}(t) \end{aligned} \quad (5)$$

where  $\mathbf{s}_{FM} = \mathbf{a}\mathbf{b}(\theta) \left[ \mathbf{W}_{FM}^H \mathbf{a}(\theta, r) \right] \boldsymbol{\phi}_{FM}(t - \tau)$  and  $\mathbf{a}_{FM}(\theta, r) = [1, \exp(-j\Theta_{FM}), \dots, \exp(-j(M-1)\Theta_{FM})]$  denotes the transmit steering vector, where  $\Theta_{FM} = 2\pi \left( \frac{d \sin \theta}{\lambda} - \frac{2r \Delta f}{c} \right)$ ,  $r$  denotes range,  $\Delta f$  is the frequency increment and  $c$  being the speed of light.  $\mathbf{W}_{FM} = \text{diag}(w)$  denotes a diagonal matrix with diagonal entries being,  $w = \frac{\mathbf{a}(\theta, r)}{\sqrt{N}}$  representing weight vector array which denotes maximum gain emission beam.  $\Theta_{FM}(t)$  denotes transmitted waveforms with dimensions  $M \times 1$ ,  $\mathbf{b}(\theta)$  denotes receive steering vector and  $\alpha$  is the echo coefficient. The subscript  $FM$  denotes FDA-MIMO.

The signal model for Dual Coprime FDA-MIMO is provided in section 3.2.

## 3 | SYSTEM MODEL

A system architecture given in Figure 2 shows the proposed cognitive Dual Coprime FDA-MIMO network target detection and tracking algorithm. The algorithm has been divided into two phases: the search phase and a tracking phase.

The initial phase of the algorithm faces the challenge of unknown target range, angle, and the presence of a deceiving main-lobe interference. To overcome this, a network of  $G$  DCFDA-MIMO radars, each with  $2N$  transmit antennas and  $M$  receive antennas having frequency increments of  $\Delta f$  and  $Q_1, Q_2, p$  being the coprime integers multiplying the frequency increments. The distance between the  $M$  antenna element is  $N_g d_m$  whereas the distance between  $N$  antenna elements is  $M_g d_n$ ,  $d_n$  and  $d_m$  being  $\frac{\lambda}{2}$ . The  $G$  radars are strategically positioned in diverse locations concurrently scan the airspace. Each radar independently estimates the target's range, angle, and potentially other parameters based on its received signals. By leveraging true target and deceptive interference signal's spatial signatures, a process called homologous detection is performed across the estimated parameters from different radars. This allows for the successful identification of the true target amidst the clutter, leading to the initialisation of its trajectory.

Following successful track initialisation, all radars transition to the tracking phase. An Extended Kalman Filter (EKF) plays a crucial role here, predicting the target's state for each individual radar. To optimise the reception of target signals while minimising interference, each radar employs a Minimum Variance Distortionless Response (MVDR) beamformer. This beamformer utilises the output of EKF to employ optimised weights to each element in the array, resulting in enhanced target detection while mitigation main-lobe interference. Using these optimised weights, the radars continuously acquire updated measurements of the target. These latest measurements are then fed back into the EKF filter to refine the predicted target state, ensuring the tracking process remains accurate. To further improve tracking accuracy and reduce individual radar errors, 2D-MUSIC Outputs of each radar as

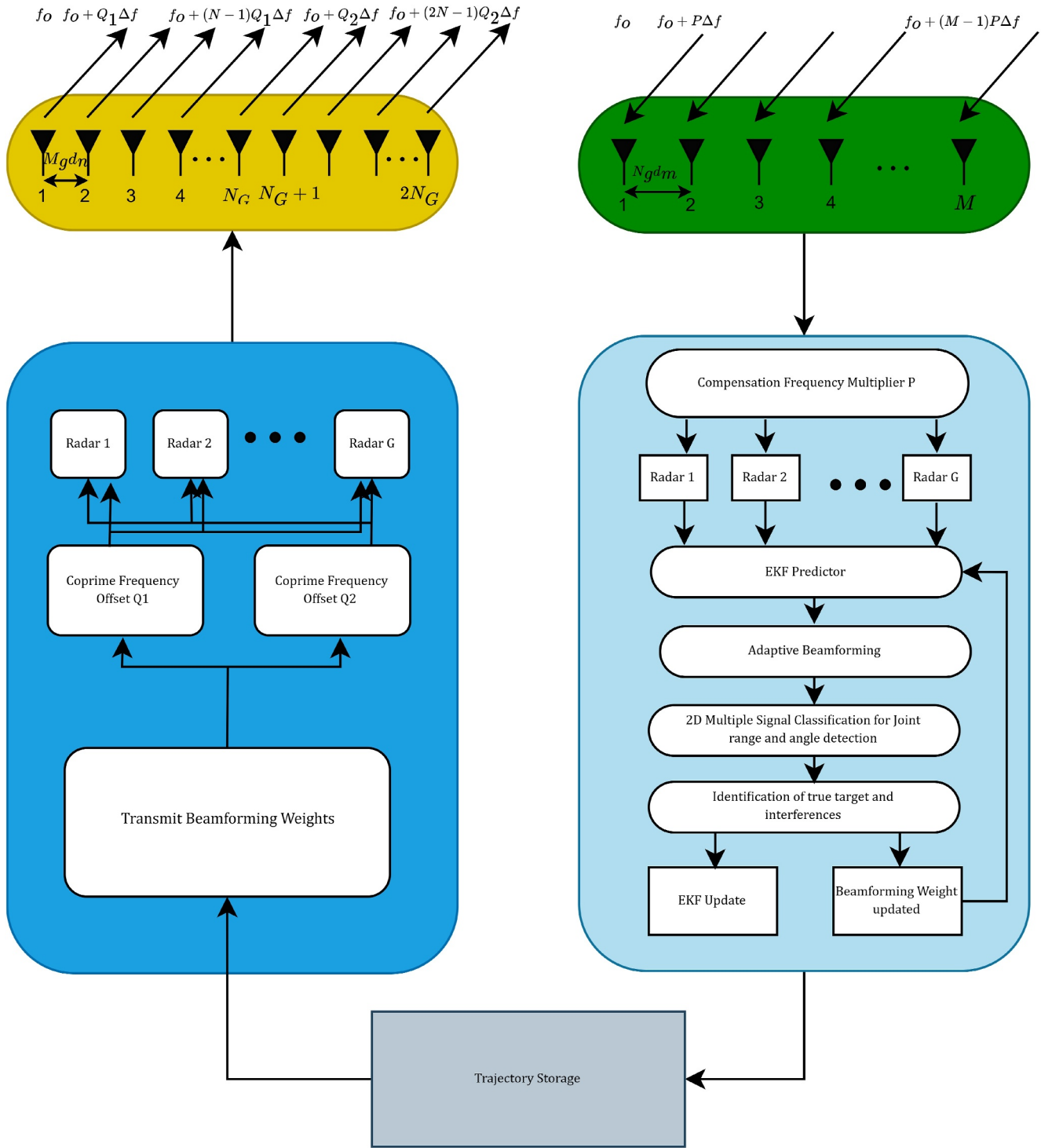


FIGURE 2 The proposed system model.

well as previous estimates are used to improve the future estimates of the true target location for the next scan cycle, and the cycle repeats.

### 3.1 | Evolution model

The model evolves with each iteration and unit as follows:

$$x_{g,k} = f_g(x_{g,k-1}, v_{g,k-1}) \tag{6}$$

The Equation (6) employs subscript  $g$  as reference to the  $g$ -th radar, and  $f_g$  to the linear/non-linear state transfer function,  $k$  is the  $k$ -th Coherent Processing Interval (CPI), and process noise denoted as  $v$ . Furthermore, the position and velocity information of the target can be given as shown in Equation (7):

$$\mathbf{x} = [x_{coord}, y_{coord}, x_{vel}, y_{vel}]^T \quad (7)$$

where subscript *coord* denotes the  $x$  and  $y$  coordinates, whereas *vel* refers to the velocity in corresponding coordinates.

### 3.2 | Signal model of target

In an investigation of a network of  $G$  co-located DCFDA-MIMO radars, a  $g$ -th radar comprises  $2 \times N_G$  transmitting elements and  $M_G$  receiving elements separated by  $d_G$  as defined in Equation (8) from adjacent array elements (Transmitter and Receiver):

$$d_G = \frac{\lambda_{R,0}}{2} \quad (8)$$

The frequency increments between the array elements are represented by  $\Delta f_g$ , whereas  $f_{g,0}$  denotes reference carrier frequency. Consequently, Equation (9) expresses the  $n$ -th element's transmitted signal as shown below:

$$f_{g,n} = f_{g,0} + nQ_1\Delta f_g \quad (9)$$

The signal transmitted by the  $n$ th element is as follows:

$$S_{(g,n)}(t) = \sqrt{\frac{E_g}{M_g}} \varphi_{g,n}(t) e^{2\pi f_{g,n} t}, 0 \leq t \leq T_g \quad (10)$$

Equation (10) defines the signal transmitted by  $n$ -th element of  $g$ -th radar whereas  $E_g$  is the energy consumed by  $g$ -th radar which is dependent on the complex envelope of the signal denoted by  $\varphi$ , and the pulse duration,  $T_g$ . Furthermore, the signal envelope satisfies an orthogonality condition, which is presented below:

$$\int_{T_g} \varphi_{g,l}(t) \varphi_{g,0}^*(t - \tau) = 0, l \neq 0, \forall \tau \quad (11)$$

where  $\tau$  denotes time shift. Considering the observable horizon range of the  $g$ -th radar being  $[0 \text{ m}, R_{g,u} \text{ m}]$ , where  $R_{g,u}$  represents the maximum unambiguous range. The observable range is further discretised to  $N_{bin}$  range bins, resulting in size of single bin as follows:

$$r_\Delta = \frac{c}{2B_w} \quad (12)$$

where  $B_w$  denotes the bandwidth.

Now consider a far field narrowband signal assumed to be impinging on the receiver array from  $(r, \theta)$ , then the  $n$ -th transmit element and  $m$ -th receiver element produce a received signal which can be shown as in Equation (13):

$$y_{g,m} = \sqrt{\frac{E}{2N_1}} \varphi_{g,n}(t - \tau_{n,m}) e^{j2\pi(f_0 + nQ_1\Delta f)(t - \tau_{n,m})} \quad (13)$$

where the time it takes for the signal to reach from the  $n$ -th element to the  $m$ -th element can be given as  $\tau_{n,m} = \frac{2r - nM_1d \sin \theta - mN_1d \sin \theta}{c}$ . Consequently, the  $m$ -th element received signal due to  $n$ -th element can be expressed as in Equation (14):

$$y_{g,m} = \rho \sum_{n=1}^{2N} \varphi_{g,n}(t - \tau_{g,n,m}) e^{j2\pi f_{g,m}(t - \tau_{g,n,m})} \quad (14)$$

$$y_{g,m} = \rho \sum_{n=1}^{2N} \varphi_{g,n}(t - \tau_{g,n,m}) e^{j\varphi_{n,m}(t')}$$

where  $\rho$ , while utilising the narrow-band assumption, denotes the complex scattering coefficient of the far field point target that is,  $\varphi_{g,m}(t - \tau_{g,n,m}) \approx \varphi_{g,m}(t - \tau_{g,0})$ , where the complex envelope stays the same for the said distance. The time  $t'$  in Equation (14) can be shown as follows:

$$\varphi_{n,m}(t') = \int_0^{t' + \frac{nM_1d \sin \theta + mN_1d \sin \theta}{c}} 2\pi(f_0 + nQ_1\Delta f) dx \quad (15)$$

The Equation (15) can be rewritten as given below:

$$\varphi_{n,m}(t') = 2\pi(f_0 t' + nQ_1\Delta f t' + \frac{f_0 d \sin \theta}{c}(nM_1 + mN_1) + \frac{nQ_1\Delta f}{c}(nM_1 d \sin \theta + mN_1 d \sin \theta)) \quad (16)$$

Since  $\Delta f \ll c$ , so  $\frac{(nQ_1\Delta f)(nM_1 d \sin \theta + mN_1 d \sin \theta)}{c}$  is small enough to be ignored, so:

$$\varphi_{n,m} = 2\pi(f_0 t' + nQ_1\Delta f t' + \frac{f_0 d \sin \theta}{c}(nM_1 + mN_1)) \quad (17)$$

The output signal after mixing the received signal with  $e^{-j2\pi f_0 t}$  can be expressed as follows:

$$\hat{s}_{n,m}(t') = \sqrt{\frac{E}{2N_1}} \varphi_{n,m}(t') e^{j(2\pi(f_0 t' + nQ_1\Delta f t' + \frac{f_0 d \sin \theta}{c}(nM_1 + mN_1)))} \quad (18)$$

whereas the phase term is rearranged as follows:

$$2\pi \left( f_0 \left( -\frac{2r}{c} \right) + nQ_1\Delta f t' + \frac{f_0 d \sin \theta}{c}(nM_1 + mN_1) \right) \quad (19)$$

The output of the  $m$ -th receive element after frequency compensation is given as follows:

$$y_{g,n,m}^{n_{bin}} = \sqrt{\frac{E}{2N_1}} \eta \varphi_{g,n,m}(t')$$

$$e^{j2\pi \left( nQ_1 \Delta f t' - f_0 \frac{2r}{c} + \frac{f_0 d \sin \theta}{c} \right) (nM_1 + mN_1)}$$
(20)

$$y_{g,n,m}^{n_{bin}} = \sqrt{\frac{E}{2N_1}} \xi \varphi_{g,n,m}(t')$$

$$e^{j2\pi \left( (nQ_1 \Delta f + mP_1 \Delta f) t' - f_0 \frac{2r}{c} + \frac{f_0 d \sin \theta}{c} \right) (nM_1 + mN_1)}$$

The  $m - th$  received signal is separated employing 2N matched filters  $\varphi_{g,n,m}(t)$  which can be given as follows:

$$\varphi_{g,n,m}(t) = e^{-j2\pi(nQ_1 \Delta f + mP_1 \Delta f)t}$$
(21)

After which, the output can be expressed as follows:

$$y_{n,m}(t) = \sqrt{\frac{E}{2N_1}} \xi e^{j2\pi \left( -f_0 \frac{2r}{c} - (nQ_1 + mP_1) \frac{2\Delta f}{c} + \frac{f_0 d \sin \theta}{c} \right) (nM_1 + mN_1)}$$
(22)

the phase term is further simplified as follows:

$$(nQ_1 \Delta f + mP_1 \Delta f) t' + (nQ_1 \Delta f + mP_1 \Delta f) t =$$

$$(nQ_1 + mP_1) \Delta f (t' - t)$$

*Since*  $t' - t = -\frac{2r}{c}$

(23)

$$(nQ_1 + mP_1) \Delta f \left( -\frac{2r}{c} \right) = -(nQ_1 + mP_1) \frac{\Delta f 2r}{c}$$

whereas  $\xi$  is the complex valued coefficient after match filtering

$$\xi_p(t) = \sqrt{\frac{E}{2N_1}} \xi(t) e^{-j2\pi f_0 \frac{2r}{c}}$$
(24)

$\mathbf{a}_k$  and  $\mathbf{b}_k$  can be expressed as follows:

$$\mathbf{a}_t(r_g, \theta_g) = \left[ 1, e^{2\pi f_{rg}}, \dots, e^{2\pi(2N_1)f_{rg}} \right]^T$$

$$\mathbf{a}_r(r_g, \theta_g) = \left[ 1, e^{2\pi f_{rg}}, \dots, e^{2\pi(2N_1)f_{rg}} \right]^T$$
(25)

whereas:

$$f_t = \left( \frac{M_1 d \sin \theta_g}{\lambda} - \frac{2r_g Q_1 \Delta f}{c} \right)$$

$$f_r = \left( \frac{N_1 d \sin \theta_g}{\lambda} - \frac{2r_g P_1 \Delta f}{c} \right)$$
(26)

whereas the phase term can be simplified as follows:

$$e^{j2\pi \left( -f_0 \frac{2r}{c} - (nQ_1 + mP_1) \frac{2\Delta f}{c} + \frac{f_0 d \sin \theta}{c} \right) (nM_1 + mN_1)}$$

$$e^{j2\pi f_t} e^{j2\pi f_r}$$
(27)

As for the Doppler frequency shift caused due a far-field target located at  $(r_g, \theta_g)$  moving with the radial velocity  $v_g$  can be denoted as follows:

$$f_{g,d} = \frac{2v_g}{\lambda_{g,0}}$$
(28)

Assuming that the  $g - th$  DCFDA-MIMO radar transmits L pulses within a single CPI, and the target's range, angle and Doppler frequency shift remain constant throughout the CPI, the signal model for the target at  $n_{bin} - th$  range bin of the  $g - th$  DCFDA-MIMO radar can be extended as follows:

$$\mathbf{X}_g^{(Sig), n_{bin}} = \xi \left( \mathbf{b}(r_g, \theta_g) \times \mathbf{a}_d(f_{g,d})^T \right) \otimes \mathbf{a}(r_g, \theta_g)$$
(29)

where

$$\mathbf{a}_d(f_{g,d}) = \left[ 1, e^{j2\pi f_{g,d} T_{CPI}}, \dots, e^{j2\pi f_{g,d} (L-1) T_{CPI}} \right]^T$$
(30)

### 3.3 | Mitigating main-lobe deception in radar tracking

One class of radar jamming techniques leverages deception strategies to generate interfering signals within the main lobe of the radar's beam pattern. This injects false target echoes into the received signal, potentially compromising target detection and tracking capabilities. This strategy involves intercepting the original radar signal, analysing its key parameters (e.g., pulse repetition frequency, modulation) and then replicating it with intentional modifications. These manipulated signals create 'ghost' targets that exhibit realistic trajectories, often mirroring the range and velocity of the true target with some degree of offset. By introducing controlled time delays, either exceeding or falling short of the original pulse period, the jammer can deliberately introduce discrepancies in the range and Doppler information associated with the false targets. This approach aims to confuse the radar receiver and impede accurate target identification and tracking.

Consider a scenario where in any CPI, the  $n_{bin} - th$  range bin contains a far field target at  $(r_g, \theta_g)$  and  $N^J$  main-lobe deceptive trajectory interference at  $(r_{g,j}, \theta_{g,j})_{j=1}^{N^J}$ , the interference signal can be modelled as follows:

$$\mathbf{X}_g^{(Jam), n_{bin}} = \sum_{j=1}^{N^J} \xi_j \left( \mathbf{b}(r_{g,j}, \theta_{g,j}) \times \mathbf{a}_d(f_{g,d,j})^T \right) \otimes \mathbf{a}(r_{g,j}, \theta_{g,j})$$
(31)

In case of main-lobe interference,  $f_{g,dj}$  and  $r_{gsj}$ , which denote the  $j$ -th false target's doppler shift and radial range with respect to the  $g$ -th radar after modulation respectively, assuming that the DRFM follows the same signal as of the true target, therefore  $\theta_j$  will reflect as such.

Following the previous analysis of jamming signals, the received signal model is modified as follows:

$$\mathbf{Y}_{g,k}^{n_{bin}} = \mathbf{X}_{g,k}^{(Sig),n_{bin}} + \mathbf{X}_{g,k}^{Jam,n_{bin}} + \mathbf{N} \quad (32)$$

where  $\mathbf{N} \in \mathbb{C}_{M_g N_g \times L}$  represents complex white Gaussian noise components with zero mean and covariance  $\sigma_g^2$ .

Then the set of signals from all range bins can be represented as follows:

$$\mathbf{Y}_{g,k} = \left\{ \mathbf{Y}_{g,k}^1, \mathbf{Y}_{g,k}^2, \dots, \mathbf{Y}_{g,k}^{N_{bin}} \right\} \quad (33)$$

## 4 | DCFDA-MIMO NETWORK

Rather than using a single radar, where a main-lobe interference suppresses the detection performance, an approach to use multiple radars has proven to be advantageous [23]. Higher resolution of DCFDA-MIMO due to its coprime frequency offset nature will enable it to distinguish between targets more precisely.

A cognitive DCFDA-MIMO network as shown in two employs a closed loop structure where a dedicated tracker estimates the target's position. This information is then used by a radar system to continuously monitor the target and provide the tracker with the latest measurements. This closed-loop feedback mechanism enhances the system's overall performance.

Multiple targets appearing in Figure 3 observed within a fixed CPI have different true angles for two radars 1 and 2.

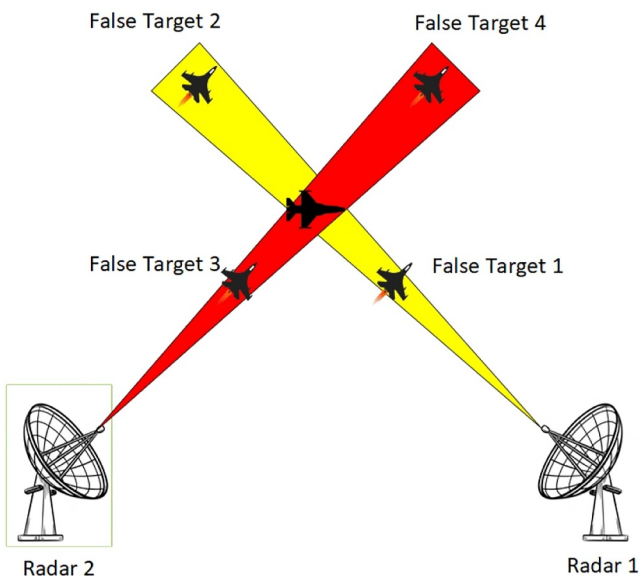


FIGURE 3 Radar network.

Thus the main-lobe interference generated will be distinguishable by the two radars in range and angle dimension.

### 4.1 | DCFDA-MIMO network for cognitive target discrimination

Suppose the range has been divided into  $N$  bins whereas there are  $G$  radars in network. For the  $n_{bin}$ -th range bin, assuming that the signal received by the  $g$ -th radar at the  $k$ -th CPI is  $\mathbf{Y}_{g,k-1}^{n_{bin}}$ , then the covariance matrix of the target-interference-noise signal for the  $g$ -th radar in the  $(k-1)$ th CPI is as follows:

$$\mathbf{R}_{g,k-1}^{n_{bin}} = \frac{1}{L} \mathbf{Y}_{g,k-1}^{n_{bin}} \mathbf{Y}_{g,k-1}^{n_{bin}H} \quad (34)$$

Following detection through 2-D MUSIC algorithm for the  $g$ -th radar at the  $(k-1)$ th CPI:

$$\hat{\mathbf{P}}_{MU}(e^{jw}) = \frac{1}{\mathbf{e}^H \mathbf{U}_N \mathbf{U}_N^H \mathbf{e}} = \frac{1}{\sum_{i=p+1}^M |\mathbf{e}^H \mathbf{v}_i|^2} \quad (35)$$

where  $\mathbf{v}_i$  are the noise eigenvectors and

$$\mathbf{e} = \left[ 1 \ e^{jw} \ e^{2jw} \ \dots \ e^{j(M-1)w} \right]^T \quad (36)$$

is the candidate steering vector. The largest peaks  $p$  of the estimation function represent the frequency estimates of the  $p$  signal components.

$$\hat{\mathbf{w}} = \underset{\mathbf{w}}{\operatorname{argmax}} \hat{\mathbf{P}}_{MU}(e^{jw}) \quad (37)$$

where  $\hat{\mathbf{w}} = \operatorname{kron}(\mathbf{b}(\hat{r}, \hat{\theta}), \mathbf{a}(\hat{r}, \hat{\theta}))$  forms the virtual steering vector and  $\theta \in [-\frac{\pi}{2}, \frac{\pi}{2}]$  and  $\hat{r} \in [(n_{bin}-1), n_{bin}] \times \left(\frac{R_{g,u}}{N_{bin}-1}\right)$

The pseudo spectrum of the  $g$ -th radar in all observation range intervals at the  $(k-1)$ th CPI is:  $\mathbf{P}_{MUSIC} = \bigcup_R \left\{ \mathbf{P}_{MUSIC}^1, \mathbf{P}_{MUSIC}^2, \dots, \mathbf{P}_{MUSIC}^{N_{bin}} \right\}$  Where  $\bigcup_R$  denotes a union of the range dimension. Constant False Alarm Rate (CFAR) detection algorithm can be applied on the obtained pseudo spectrum  $P_{MUSIC}$  and in case of high Signal to Noise Ratio (SNR) and high interference to noise ratio (INR), the algorithm is able to reliably extract the range and angle information of the target and interference

$$\mathbf{Z}_{g,k-1} = \mathbf{Z}_{g,k-1}^T \cup \mathbf{Z}_{g,k-1}^F = \left\{ z_{g,k-1}^n \right\}_{\tilde{N}_{g,k-1}} \quad (38)$$

The relationship between target location, velocity and range and angle can be modelled as non-linear functions:

$$\begin{bmatrix} r \\ \theta \end{bmatrix} = \mathcal{H}(x) + \mathcal{V} = \begin{bmatrix} \sqrt{x_l^2 + y_l^2} \\ \arctan\left(\frac{y_l}{x_l}\right) \end{bmatrix} + \mathcal{V} \quad (39)$$



where  $\mathcal{V}$  denotes the measurement noise and  $\mathcal{G}(\cdot)$  denotes the nonlinear measurement function.

The measurement set acquired simultaneously across  $G$  radars at the same CPI can be denoted as follows:

$$\mathbf{Z}_{k-1} = \{\mathbf{z}_{g,k-1}\}_{g=1}^G \quad (40)$$

The difference between measurements of any two radars is represented by Euclidean distance matrix and is defined as follows:

$$D_{g\hat{g}} = \begin{bmatrix} d_{11} & d_{12} & \cdots & d_{1\tilde{N}_{\hat{g},k-1}} \\ d_{21} & d_{22} & \cdots & d_{2\tilde{N}_{\hat{g},k-1}} \\ \vdots & \vdots & \ddots & \vdots \\ d_{\tilde{N}_{g,k-1}1} & d_{\tilde{N}_{g,k-1}2} & \cdots & d_{\tilde{N}_{g,k-1}\tilde{N}_{\hat{g},k-1}} \end{bmatrix} \quad (41)$$

where  $D_{g\hat{g},k-1} \in \mathbb{C}^{\tilde{N}_{g,k-1} \times \tilde{N}_{\hat{g},k-1}}$

Also  $d_{sl} = E\left(\mathcal{G}^{-1}\left(\mathbf{z}_{g,k-1}^s\right), \mathcal{G}^{-1}\left(\mathbf{z}_{\hat{g},k-1}^l\right)\right)$  Where  $E$  is the Euclidean Distance operator,  $g$  and  $\hat{g}$  represent the  $g$ -th and  $\hat{g}$ -th radars.

An indicator matrix  $\{0, 1\}$  is established according to the distance threshold  $\zeta$  and the Euclidean distance matrix  $D_{g\hat{g},k-1}$ . Here, 1 represents the true target and 0 represents the false target.

$$\begin{bmatrix} \mathcal{L}(d_{11}) & \mathcal{L}(d_{12}) & \cdots & \mathcal{L}\left(d_{1\tilde{N}_{\hat{g},k-1}}\right) \\ \mathcal{L}(d_{21}) & \mathcal{L}(d_{22}) & \cdots & \mathcal{L}\left(d_{2\tilde{N}_{\hat{g},k-1}}\right) \\ \vdots & \vdots & \ddots & \vdots \\ \mathcal{L}\left(d_{\tilde{N}_{g,k-1}1}\right) & \cdots & \cdots & \mathcal{L}\left(d_{\tilde{N}_{g,k-1}\tilde{N}_{\hat{g},k-1}}\right) \end{bmatrix} \quad (42)$$

where  $\mathcal{L}(d_{sl}) = \begin{cases} 1, & d_{sl} < \zeta \\ 0, & d_{sl} \geq \zeta \end{cases}$

The threshold  $\mathcal{L}(d_{sl})$  is applied to the acquired Euclidean distance between individual targets detected by both of radars, respectively. Specifically, if the distance between two targets is below the threshold, it signifies that the two targets are essentially the same.

The indicator matrix  $\hat{D}_{g\hat{g},k-1}$ , then helps identification of true target from the deceptive interference found in main-lobe.

### 4.2 | Cognitive DCFDA-MIMO network target tracking aided with EKF

The target state is initialised by using utilising the output of 2D-MUSIC from each radar and target covariance matrix. After initialising the target state, the predicted state can be continuously sent to the radar system. Combining the tracker output with the radar 2-D MUSIC output of the  $g - th$  and

$g' - th$  radar, the tracker performance can be improved to provide more accurate predicted target state.

Assuming that  $N_I$  CPIs reare initialise to correctly initialise the tracker for  $g - th$ , now representing the state as  $x_{g,k-1+N_I}$ , in which, be rewriting  $(k - 1 + N_I)$  as  $k - 1$ , we can write  $x_{g,k-1+N_I}$  as  $x_{g,k-1}$ . Then the predicted state for the  $k$ -th CPI can be written as follows:

$$x_{(g,k|k-1)} = \mathbf{F}x_{g,k-1} + \mathbf{v} \quad (43)$$

here process noise with 0 mean and covariance matrix  $\mathbf{Q}$  is denoted as  $\mathbf{v}$ , whereas a transition matrix of linear nature is denoted as  $\mathbf{F}$ .

$$\mathbf{F} = \alpha \begin{bmatrix} \mathbf{I}_2 & \mathbf{T}_{\text{CPI}}\mathbf{I}_2 \\ \mathbf{0}_2 & \mathbf{I}_2 \end{bmatrix} \quad (44)$$

where  $\mathbf{I}_n$  and  $\mathbf{0}_n$  denote the  $n \times n$  identity and zero matrices

$$\mathbf{Q} = \alpha \begin{bmatrix} \frac{\mathbf{T}_{\text{CPI}}^3\mathbf{I}_2}{4} & \frac{\mathbf{T}_{\text{CPI}}^3\mathbf{I}_2}{4} \\ \mathbf{T}_{\text{CPI}}^4\mathbf{I}_2 & \mathbf{T}_{\text{CPI}}^2\mathbf{I}_2 \end{bmatrix} \quad (45)$$

where the level of process noise is controlled by manipulating  $\alpha$ . Furthermore, covariance matrix also needs to be predicted by EKF. Assuming that the target state covariance matrix for the  $g - th$  radar at  $(K - 1) - th$  CPI can be initialised to  $\mathbf{P}_{g,k-1}$ , then the covariance matrix for the  $g$ -th CPI can be predicted as follows:

$$\mathbf{P}_{(g,k|k-1)} = \mathbf{F}\mathbf{P}_{g,k-1}\mathbf{F}^T + \mathbf{Q} \quad (46)$$

### 4.3 | Range and angle prediction with 2-D MUSIC

Different from existing FDA-MIMO radar, the Dual Coprime FDA-MIMO recognises more targets against the number of antenna elements. The range and angle information can be used to suppress interference at greater number of locations compared to FDA-MIMO. With the knowledge of predicted target state, adaptive matched filters for range as well as angle dimension can be made to mitigate deceptive interference caused in the main-lobe deceptive interference, which in turn will help to recognise the true target in range-angle dimensions. Suppose the predicted state of the target by  $g - th$  radar in the  $K - th$  CPI is  $x_{(g,k|k-1)}$ , the predicted range and angle information  $\{r_{(g,k|k-1)}, \theta_{(g,k|k-1)}\}$  can be extracted using  $P_{\text{MUSIC}}$ .

Leveraging  $r_{(g,k|k-1)}, \theta_{(g,k|k-1)}$  that is, predicted range and angle, can be utilised for  $g - th$  in  $k - th$  CPI as the prior information. MVDR can be designed according to the  $n_{bin} - th$  range bin if the predicted range  $r_{(g,k|k-1)}$  falls within it. MVDR for the aforesaid range bin can be given as follows:

$$\begin{cases} \min_{\tilde{\mathbf{w}}} \tilde{\mathbf{w}}^H \mathbf{R}_{g,k} \tilde{\mathbf{w}} \\ s.t. \tilde{\mathbf{w}}^H \tilde{\mathbf{v}}(r_{(g,k|k-1)}, \theta_{(g,k|k-1)}) = 1 \end{cases} \quad (47)$$

where interference and noise while excluding  $n_{bin} - \frac{N_e}{2}$ ,  $n_{bin} + \frac{N_e}{2}$   $tb$  range bin form the  $\mathbf{R}_{g,k}$  covariance matrix. Here  $N_e$  denote the adjacent range bins to  $n_{bin} - tb$  range bin.  $\tilde{\mathbf{w}}$  determines the weight vector whereas virtual steering vector  $\tilde{\mathbf{v}}$  is given by the following:

$$\begin{aligned} \tilde{\mathbf{v}}(r_{(g,k|k-1)}, \theta_{(g,k|k-1)}) &= \mathbf{b}(r_{(g,k|k-1)}, \theta_{(g,k|k-1)}) \otimes \\ \mathbf{a}(r_{(g,k|k-1)}, \theta_{(g,k|k-1)}) \end{aligned} \quad (48)$$

By employing the predicted virtual steering vector  $\mathbf{v}(r, \theta)$  acquired for CPI  $k$ , the MVDR beamformer can be represented as follows:

$$\begin{cases} \min_{\mathbf{w}} \mathbf{w}^H \mathbf{R}_{g,k} \mathbf{w} \\ s.t. \mathbf{w}^H \mathbf{v}(r, \theta) = 1 \end{cases} \quad (49)$$

where  $\mathbf{w}$  represents the optimal weight vector. If  $\theta$  and  $r$  correspond to the  $n_\theta - tb$  the angle and the  $n_{bin} - tb$  range cells, the above weight vector  $\mathbf{w}$  applied to the received signal will give the output as follows:

$$P_{n_{bin}, n_\theta} = \left| \mathbf{w}^H \mathbf{R}_{g,k}^{n_{bin}} \mathbf{w} \right| \quad (50)$$

#### 4.4 | Target tracking

Target tracking takes place by observing the angle domain divided into  $N_\theta$  according to  $\theta_\Delta$  intervals by utilising the following:

$$\begin{cases} \min_{\tilde{\mathbf{w}}} \tilde{\mathbf{w}}^H \mathbf{R}_{g,k} \tilde{\mathbf{w}} \\ s.t. \tilde{\mathbf{w}}^H \tilde{\mathbf{v}}(r_{(g,k|k-1)}, \theta_{(g,k|k-1)}) = 1 \end{cases} \quad (51)$$

Traversing through all angles allows for the acquisition of the weight vector at each specific orientation. This process ultimately leads to the determination of the filtered output across all range bins and angular cells.

$$\mathbf{P} = \{P_{n_{bin}, n_\theta}\}; n_{bin} = 1, 2, \dots, N_{bin}, n_\theta = 1, 2, \dots, N_\theta \quad (52)$$

Upon applying a weighted filter to the output, the detection of true targets within specific ranges and angles is facilitated, while simultaneously suppressing main-lobe deceptive jamming signals. The target's location information can be extracted from  $p$  by selecting its maximum value, which can be recorded as range and angle in the following manner:

$$\mathbf{z}_{g,k} = [\tilde{r}, \tilde{\theta}] \quad (53)$$

#### 4.5 | EKF update

The latest measurements received at CPI  $k$  will be used to update the predicted target state and its covariance matrix as follows:

$$\mathbf{x}_{g,k} = \mathbf{x}_{(g,k|k-1)} + \mathbf{K}_{g,k} (\mathbf{z}_{g,k} - \mathcal{H}(\mathbf{x}_{(g,k|k-1)})) \quad (54)$$

$$\mathbf{P}_{g,k} = (\mathbf{I} - \mathbf{K}_{g,k} \mathbf{H}_{g,k}) \mathbf{P}_{(g,k|k-1)} \quad (55)$$

where  $\mathbf{K}_{g,k}$  denotes the Kalman gain as follows:

$$\mathbf{K}_{g,k} = \mathbf{P}_{(g,k|k-1)} \mathbf{H}_{g,k}^T \mathbf{S}_{g,k}^{-1} \quad (56)$$

where  $\mathbf{S}_{g,k}$  is the innovation term covariance matrix  $(\mathbf{z}_{g,k} - \mathcal{H}(\mathbf{x}_{(g,k|k-1)}))$ , whereas  $\mathcal{H}(\cdot)$  represents is the measurement function as follows:

$$\mathbf{S}_{g,k} = \mathbf{H}_{g,k} \mathbf{P}_{(g,k|k-1)} \mathbf{H}_{g,k}^T + \mathbf{R}_{g,k} \quad (57)$$

where  $\mathbf{H}_{g,k} = \frac{\delta \mathcal{H}(\mathbf{x}_{(g,k|k-1)})}{\delta (\mathbf{z}_{g,k})}$  is the  $g - tb$  radar jacobian matrix and  $\mathbf{R}_{g,k}$  denotes the measurement covariance matrix, defined as follows:

$$\mathbf{R}_{g,k} = \text{diag} \left( \begin{bmatrix} N_{r_\Delta} r_\Delta \\ N_{\theta_\Delta} \theta_\Delta \end{bmatrix}^2 \right) \quad (58)$$

where  $\theta_\Delta$  and  $r_\Delta$  denote the angular search intervals and range bin length, respectively. The selections of  $N_{r_\Delta}$  and  $N_{\theta_\Delta}$  influence the level of measurement noise.

## 5 | NUMERICAL EXPERIMENTS AND RESULTS

### 5.1 | Experimental environment

The experimental environment is set up of two radars at coordinates  $[0 \text{ m}, 0 \text{ m}]$  and  $[4000 \text{ m}, 0 \text{ m}]$  with respect to the origin, SNR at 30 dB and INR at 10 db. Two targets are introduced at  $[2000 \text{ m}, 2000 \text{ m}]$  and  $[3500 \text{ m}, 3500 \text{ m}]$  from the origin. These two DCFDA-MIMO radars have identical parameters unless specified otherwise. The number of transmit and receive elements is  $N = 3$ ,  $M = 4$  indicating a total of  $2N + M = 10$  elements, whereas speed of light is  $c = 3 \times 10^8 \text{ m/s}$ . The carrier frequency is set to  $f_o = 1 \times 10^9 \text{ Hz}$ , the  $\Delta f = 25 \times 10^3 \text{ Hz}$ , the wavelength  $\lambda = c/f_o$ , the inter-element spacing of the  $N$  transmitting array elements is  $Md$ , whereas the spacing between  $M$  receiving elements is  $Nd$  where  $d = \lambda/2$ .

### 5.2 | Experiment 1

Experiment 1 involves one interference in each of the radar's main lobe. The source of interference here being DRFM. The projected signal by the DRFM follows the same angle as the

target in main lobe. The scenario is depicted in the Figure 4 below.

Firstly, in the search phase, 2D-MUSIC is applied to find the targets and interference in the horizon, output of radar 1 followed by application of CFAR detection algorithm is shown in the Figure 5.

It is apparent in the figure that the radar is able to clearly discriminate two targets in this scenario. Moreover, a similar output of radar two is given in Figure 6.

The detected targets and interference outputs of Radar 1 and 2 are used and discriminated using distance matrix and true target is identified. Furthermore, the true target position is utilised as input for EKF to update its predictor. The EKF performance measured over 30 CPIs for radar 1's performance is show in Figure 7a,b show the radar 1 performance relating to X and Y coordinate tracking whereas Figure 7c,d show the radar 2's performance.

After updating EKF predictor, the predicted values are used for training beamforming weights for the Radar 1 and 2 according to the predicted target location. The training of the beamforming weights is achieved using CVX Convex optimisation tool. Beamforming patterns are shown in Figure 8.

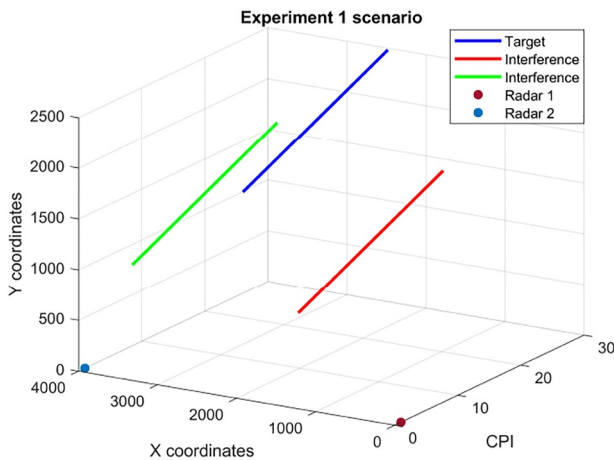


FIGURE 4 Radar experiment scene 1.

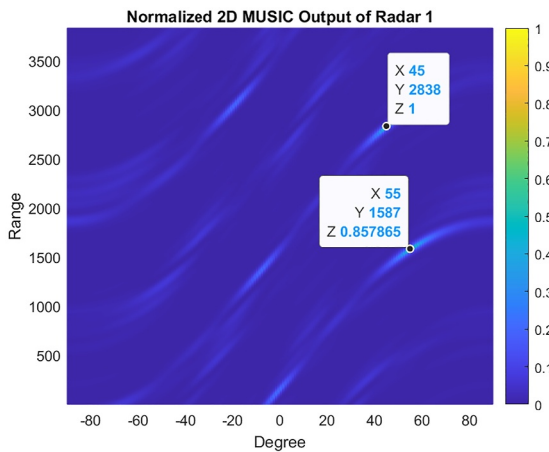


FIGURE 5 Normalised 2D-MUSIC output of radar 1 at CPI 2.

Figure 8 illustrates the beamforming capabilities of Radars 1 and 2, respectively. Specifically In Figure 8a,c,e, Radar 1 steers a beam towards the target location, which has been indicated by the maxima on the z-axis. Notably, it places a null towards the interference locations (for CPI 20, 25, and 30). Similarly, Figure 8b,d,f depict the beam steering of Radar 2 towards the same target represented with a maxima on the z-axis. Likewise, nulls have also been placed towards the interferences.

### 5.3 | Experiment 2

Experiment 2 involves 2 targets as well as increased number interference as two in each of the radar's main lobe. The interference signal here are two target projections possibly produced by DRFM. The projections follow the same angle as the target in main lobe. The scenario is depicted in Figure 9. It

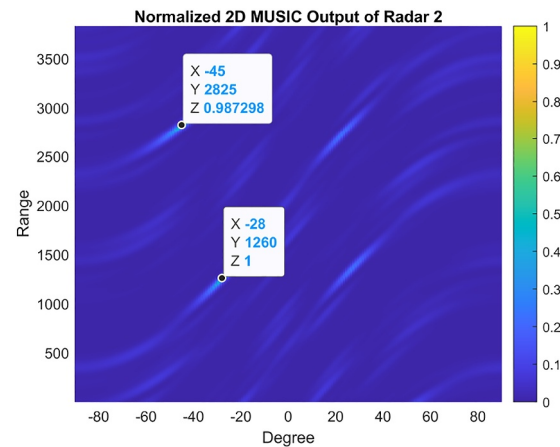


FIGURE 6 Normalised 2D-MUSIC output of radar 2 at CPI 2.

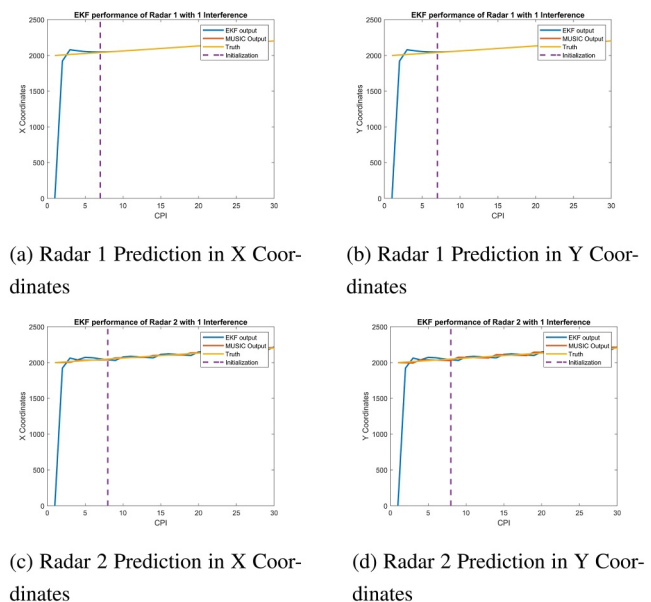


FIGURE 7 Extended Kalman Filter performance of radar 1 and 2.

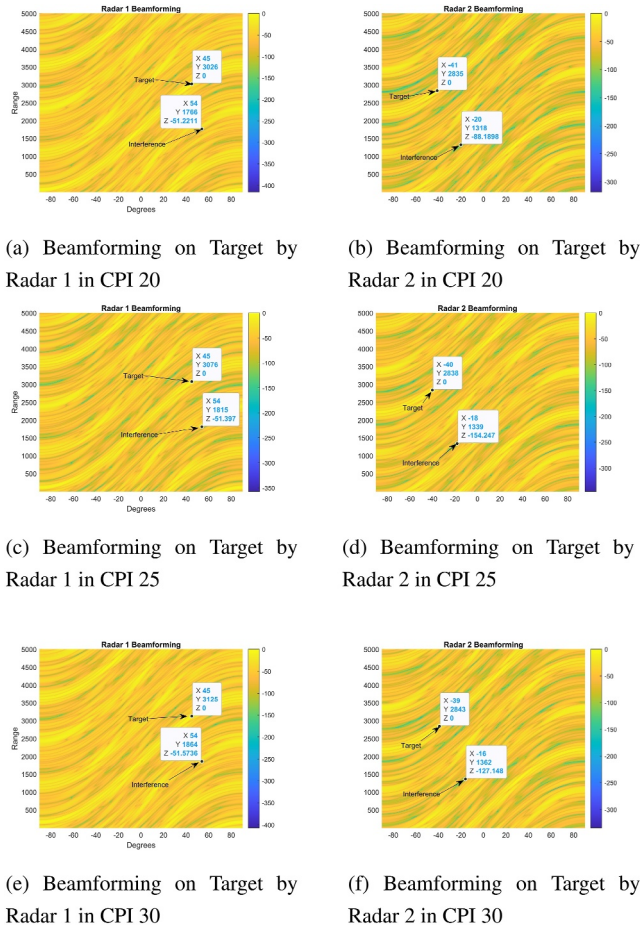


FIGURE 8 Radar beamforming with radars 1 and 2.

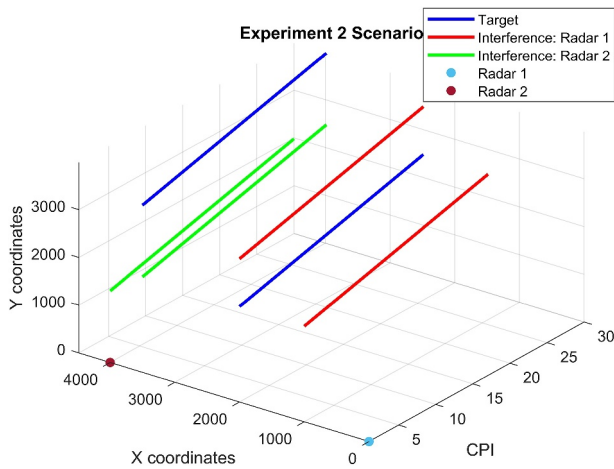


FIGURE 9 Radar experiment scene 2.

is evident that the system is robust towards more interference and can accurately track the true target even with significantly fewer number of elements compared to the FDA-MIMO Network.

2D-MUSIC outputs of the Radar 1 and 2 are given in Figures 10 and 11. It is evident that radars are able to clearly distinguish different signals in the horizon.

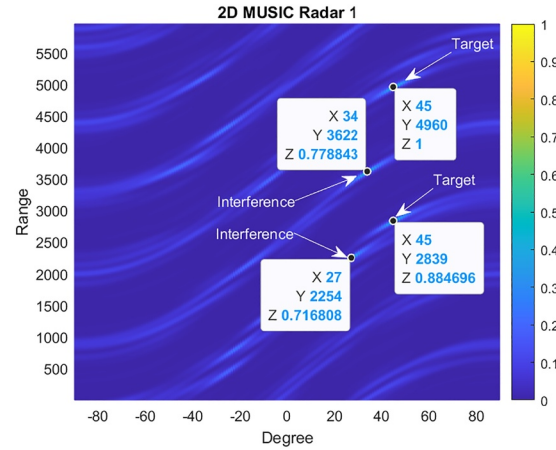


FIGURE 10 Normalised 2D-MUSIC output of radar 1 at CPI 2.

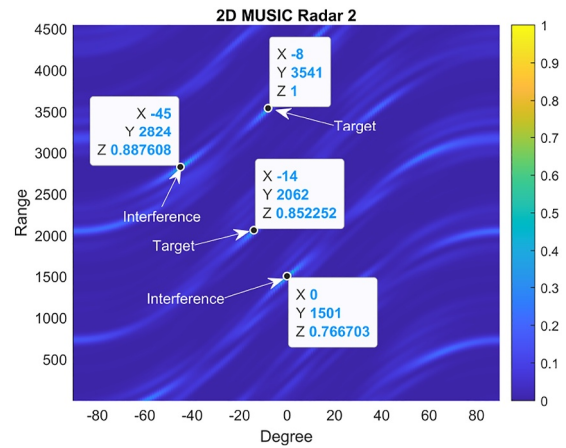


FIGURE 11 Normalised 2D-MUSIC output of radar 2 at CPI 2.

Target position prediction by EKFs for radar 1 and 2 are given in Figure 12a,b show radar 1's performance in X and Y coordinates while Figure 12c,d show radar 2's performance in the same. Likewise, beamforming outputs of radar 1 and 2 are given in Figure 13a,c,e, where Radar 1's beam is focused on target closest to its position showing higher peaks whereas producing nulls at the 2 points of interferences. Moreover, Figure 13b,d,f shows the Radar 2's beam focused on the target closest to its position with higher peaks while suppressing points of interferences in its main lobe.

It is apparent in the figures that the Beamforming focuses the beam on the target closest to them whereas producing null at the point of interference at CPI 20, 25 and 30.

In a comparison made in Figure 14 between FDA, FDA-MIMO and DCFDA-MIMO, FDA Beamformer in Figure 14a,b shows a straight beam that highlights the target. While on the other hand, FDA-MIMO beamformer in Figure 14c,d, is more focused around the target. Different from FDA and FDA-MIMO, the DCFDA-MIMO beamformer in Figure 14e,f produces a more focused area around the target resulting in a narrower beam than FDA and FDA-MIMO beamformers.

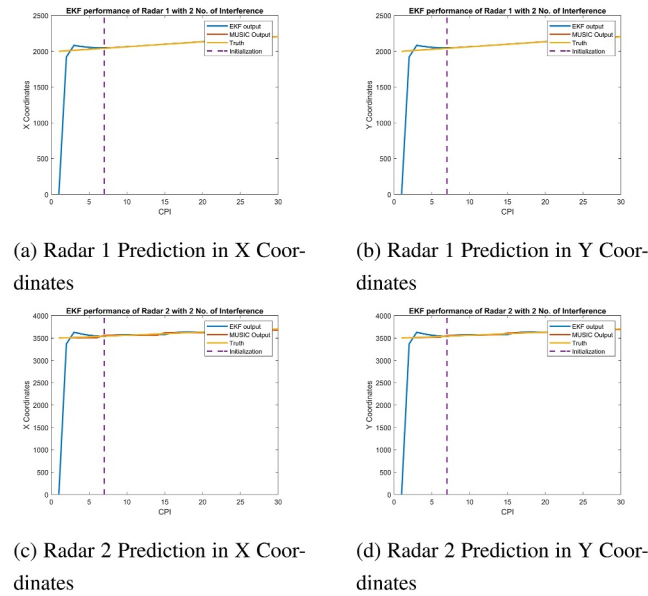


FIGURE 12 Extended Kalman Filter performance of radar 1 and 2.

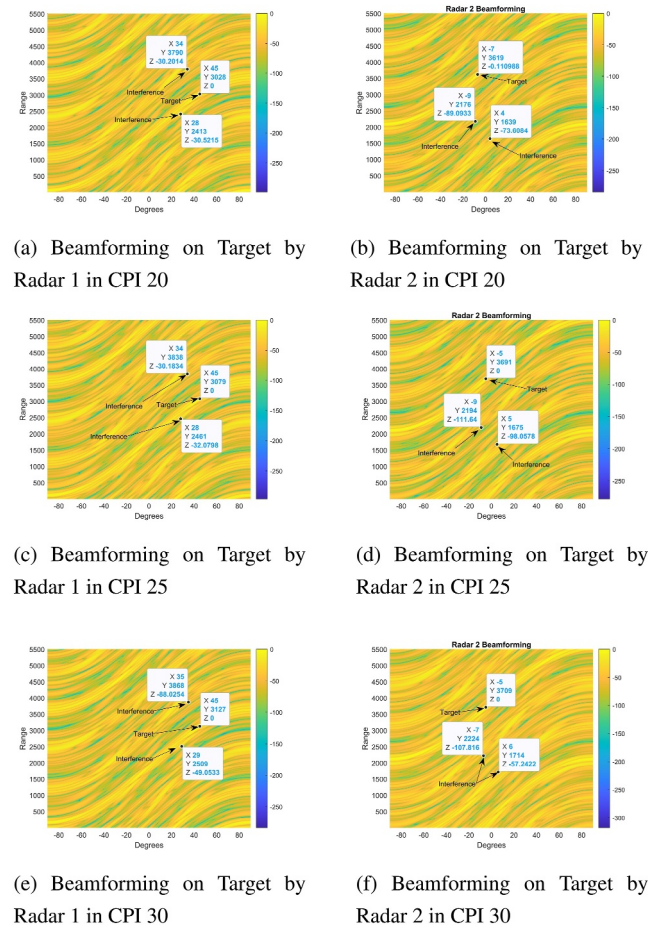


FIGURE 13 Radar beamforming with radars 1 and 2.

Furthermore, a comparison of EKF tracking using FDA-MIMO against EKF tracking using DCFDA-MIMO is given in Figure 15a which shows radar 1 performance comparison

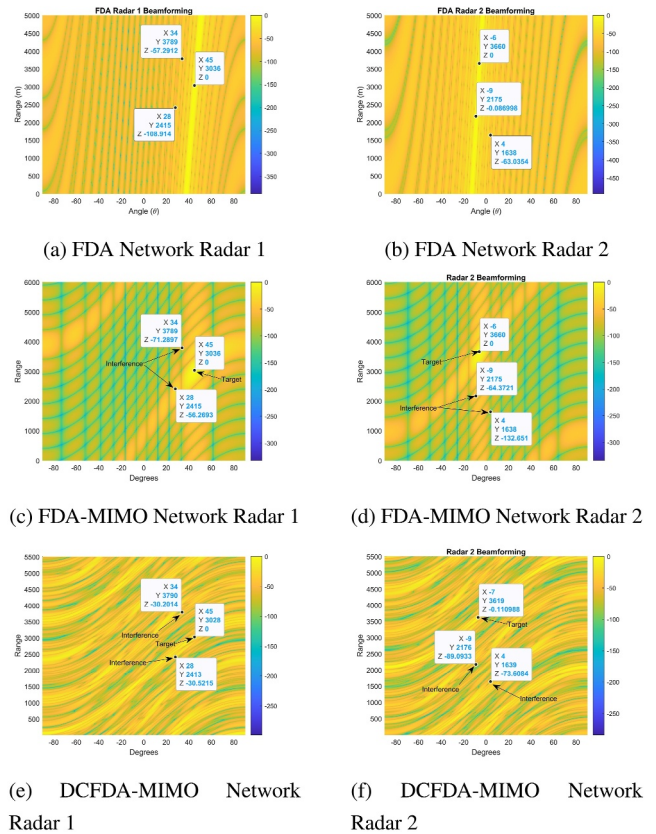


FIGURE 14 Radar Beamforming comparison between frequency diverse array (FDA), FDA-MIMO and DCFDA-MIMO.

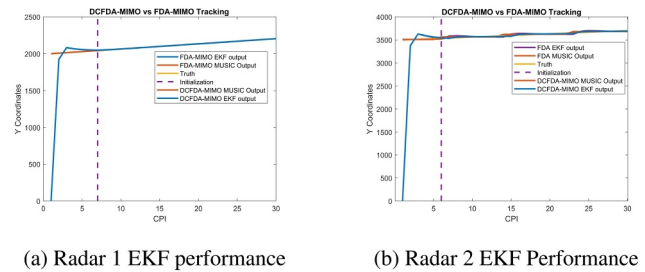


FIGURE 15 Extended Kalman Filter comparison between DCFDA-MIMO and FDA-MIMO at CPI 30 in Y coordinates.

between DCFDA-MIMO and FDA-MIMO network, whereas Figure 15b shows the same for radar 2. It is apparent that despite having lower count of elements in transmitting and receiving array, DCFDA-MIMO is able to achieve the same results as FDA-MIMO with greater number of array elements.

## 6 | CONCLUSION

We proposed a DCFDA-MIMO Network based target discrimination and tracking method, which utilises Dual Coprime FDA multiple input multiple output network for initial detection of targets and interference. Next, target discrimination is carried out to optimise beamforming weights for better

detection of targets. Experiments applying DCFDA-MIMO for mitigation of main-lobe interference has yielded the following conclusions:

1. DCFDA-MIMO radar network works with fewer elements to achieve the same results as FDA-MIMO Radar Network.
2. DCFDA-MIMO radar network can more effectively distinguish genuine targets from deceptive trajectory interference in the main lobe.
3. The main lobe of the beam pattern directs towards the genuine target while simultaneously suppressing interference.
4. EKF in combination with DCFDA-MIMO network ensures correct path of the true target.

In future work, we plan to utilise the said array for moving platform by incorporating algorithms to counter clutter interference mitigation. Furthermore, we will use radar network to focus the power towards multiple targets at the same time.

### AUTHOR CONTRIBUTIONS

**Umair Hafeez Khan:** Conceptualization; investigation; methodology; software; visualization; writing – original draft. **Abdul Basit:** Supervision; writing – review & editing. **Wasim Khan:** Supervision. **Muhammad Adeel Khan Jadoon:** Methodology. **Nauman Anwar Baig:** Conceptualization; resources; writing – review & editing.

### ACKNOWLEDGEMENTS

The Corresponding Author's institution or funder has an existing agreement (pre -paid open access account) with Wiley and may pay the Article Publication Charge from this account on behalf of the author Institution Code: K065 7.

### CONFLICT OF INTEREST STATEMENT

There are no conflicts of interest between the authors of this manuscript.

### DATA AVAILABILITY STATEMENT

The data that support the findings of this study are available from the corresponding author upon reasonable request.

### ORCID

*Umair Hafeez Khan*  <https://orcid.org/0009-0006-9483-8462>

### REFERENCES

1. Milne, K.: Phased arrays in radar. In: IEE Tutorial Meeting on Phased Array Radar, pp. 2–1. IET. London, UK (1989)
2. Lin, F.-L., Kretschmer, F.: Angle measurement in the presence of main-beam interference. *IEEE Aero. Electron. Syst. Mag.* 5(11), 19–25 (1990). <https://doi.org/10.1109/62.63159>
3. Lin, F.-L.C., Kretschmer Jr, F.F.: Performance of an angle-of-arrival estimator in the presence of a mainbeam interference source (1991). Naval Research Lab Washington Dc, Tech. Rep
4. Hassanien, A., Vorobyov, S.A.: Phased-mimo radar: a tradeoff between phased-array and mimo radars. *IEEE Trans. Signal Process.* 58(6), 3137–3151 (2010). <https://doi.org/10.1109/tsp.2010.2043976>
5. Antonik, P., et al.: Frequency diverse array radars. In: 2006 IEEE Conference on Radar, pp. 3. IEEE. Verona, NY, USA (2006)
6. Antonik, P.: An Investigation of a Frequency Diverse Array. Ph. D. dissertation. UCL (University College London). London, UK (2009)
7. Nusenu, S.Y., Basit, A.: Frequency diverse array antennas: from their origin to their application in wireless communication systems. *Journal of Computer Networks and Communications* 2018, 1–12 (2018). <https://doi.org/10.1155/2018/5815678>
8. Sun, Y., et al.: Doa estimation and tracking for fda-mimo radar signal. *Digit. Signal Process.* 106, 102858 (2020). <https://doi.org/10.1016/j.dsp.2020.102858>
9. Tan, Z., Eldar, Y.C., Nehorai, A.: Direction of arrival estimation using co-prime arrays: a super resolution viewpoint. *IEEE Trans. Signal Process.* 62(21), 5565–5576 (2014). <https://doi.org/10.1109/tsp.2014.2354316>
10. Zhang, Y.D., Qin, S., Amin, M.G.: Doa estimation exploiting coprime arrays with sparse sensor spacing. In: 2014 IEEE International Conference on Acoustics, Speech and Signal Processing (ICASSP), pp. 2267–2271. IEEE. Florence, Italy (2014)
11. Baxter, W., Nosrati, H., Aboutanios, E.: Coprime beamforming: fast estimation of more sources than sensors. *IET Radar, Sonar Navig.* 13(11), 1956–1962 (2019). <https://doi.org/10.1049/iet-rsn.2018.5647>
12. Mao, Z., et al.: Cramér-rao bound of joint doa-range estimation for coprime frequency diverse arrays. *Rem. Sens.* 14(3), 583 (2022). <https://doi.org/10.3390/rs14030583>
13. Haykin, S.: Cognitive radar: a way of the future. *IEEE Signal Process. Mag.* 23(1), 30–40 (2006). <https://doi.org/10.1109/msp.2006.1593335>
14. Martone, A.F.: Cognitive radar demystified. *URSI Radio Science Bulletin* 2014, 10–22 (2014)
15. Guerci, J.R.: Cognitive radar: a knowledge-aided fully adaptive approach. IEEE, pp. 1365–1370. Arlington, VA, USA (2010). <https://doi.org/10.1109/radar.2010.5494403>
16. Sagayaraj, M.J., et al.: A hybrid approach to cognition in radars. *Defence Sci. J.* 68(2), 183 (2018). <https://doi.org/10.14429/dsj.68.12228>
17. Nusenu, S.Y., Basit, A.: Cognitive transmit subarray fda design for integrated radar-communication using flexible sidelobe control. In: 2018 IEEE 7th International Conference on Adaptive Science & Technology (ICAST), pp. 1–6. IEEE. Accra, Ghana (2018)
18. Ding, Z., Xie, J., Yang, L.: Cognitive conformal subaperturing fda-mimo radar for power allocation strategy. *IEEE Trans. Aero. Electron. Syst.*, 1–13 (2023). <https://doi.org/10.1109/taes.2023.3247978>
19. Roome, S.: Digital radio frequency memory. *Electron. Commun. Eng. J.* 2(4), 147–153 (1990). <https://doi.org/10.1049/ecej:19900035>
20. Berger, S.D., Meer, D.E.: An expression for the frequency spectrum of a digital radio frequency memory signal. In: IEEE Conference on Aerospace and Electronics, pp. 90–93. IEEE (1990)
21. Zhong, H., Wang, F., Zhou, J.: Performance analysis of active cancellation system based on drfm. In: 2018 IEEE 4th International Conference on Computer and Communications (ICCC), pp. 1228–1233. IEEE (2018)
22. Wei, L., et al.: Drfm range false target cancellation method based on slope-varying lfm chirp signal. In: 2016 IEEE 13th International Conference on Signal Processing (ICSP), pp. 1629–1632. IEEE (2016)
23. Yang, B., et al.: Cognitive fda-mimo radar network for target discrimination and tracking with main-lobe deceptive trajectory interference. *IEEE Trans. Aero. Electron. Syst.* 59(4), 4207–4222 (2023). <https://doi.org/10.1109/taes.2023.3237663>
24. Xu, J., et al.: Deceptive jamming suppression with frequency diverse mimo radar. *Signal Process.* 113, 9–17 (2015). <https://doi.org/10.1016/j.sigpro.2015.01.014>
25. Lan, L., et al.: Suppression of mainbeam deceptive jammer with fda-mimo radar. *IEEE Trans. Veh. Technol.* 69(10), 11584–11598 (2020). <https://doi.org/10.1109/tvt.2020.3014689>
26. Lan, L., et al.: Beampattern synthesis based on novel receive delay array for mainlobe interference mitigation. *IEEE Trans. Antenn. Propag.* 71(5), 4470–4485 (2023). <https://doi.org/10.1109/tap.2023.3247916>

27. Lan, L., et al.: Grlt-based adaptive target detection in fda-mimo radar. *IEEE Trans. Aero. Electron. Syst.* 57(1), 597–613 (2020). <https://doi.org/10.1109/taes.2020.3028485>
28. Gong, P., Wu, Y.: Improved transmit beamforming design based on admm for low probability of intercept of fda-mimo radar. *J. Commun.* 43(4), 133–142 (2022)
29. Gong, P., et al.: Joint design of transmit waveform and receive beamforming for lpi fda-mimo radar. *IEEE Signal Process. Lett.* 29, 1938–1942 (2022). <https://doi.org/10.1109/lsp.2022.3205206>
30. Gong, P., et al.: Optimization of lpi-fda-mimo radar and mimo communication for spectrum coexistence. *IEEE Wireless Communications Letters* 12(6), 1076–1080 (2023). <https://doi.org/10.1109/lwc.2023.3261419>
31. Wang, W.-Q., So, H.-C.: Transmit subaperturing for range and angle estimation in frequency diverse array radar. *IEEE Trans. Signal Process.* 62(8), 2000–2011 (2014). <https://doi.org/10.1109/tsp.2014.2305638>

**How to cite this article:** Khan, U.H., et al.: Cognitive dual coprime frequency diverse array MIMO radar network for target discrimination and main-lobe interference mitigation. *IET Radar Sonar Navig.* 18(9), 1584–1597 (2024). <https://doi.org/10.1049/rsn2.12595>